Journal of Applied Polymer Science

Toughening Effects of Nucleating Agent on Impact Polypropylene Copolymer

Miaomiao Sun, Dali Gao, Hongbo Zhang, Hao Zou, Meng Xu, Shijun Zhang, Jie Li, Jianye Liu
Beijing Research Institute of Chemical Industry, Beijing 100013, People's Republic of China
Correspondence to: H. Zou (E-mail: zouh.bjhy@sinopec.com)

ABSTRACT: In this study, the impact polypropylene copolymer (IPC) blended with the sorbitol-based nucleating agent (NA) NX8000 was prepared and then characterized using a wide range of instrumentations. The results showed that the NA formed a fibril network which resulted in the increased viscosity of system and the decreased size of ethylene–propylene random copolymer (EPR) phase. The results of mechanical tests revealed "the brittle–ductile transition (BDT)" occurred while the ethylene content was between 3.5 wt % and 6 wt % and indicated that the impact strength of IPC was greatly improved by the addition of NX8000 when the EPR content was right over the critical value of BDT. The investigations provided valuable information for the further development of IPC materials and boarded its potential industrial applications. © 2014 Wiley Periodicals, Inc. J. Appl. Polym. Sci. **2014**, *131*, 40705.

KEYWORDS: copolymers; mechanical properties; morphology

Received 7 November 2013; accepted 21 February 2014
DOI: 10.1002/app.40705

INTRODUCTION

Impact polypropylene copolymer (IPC) is a new polypropylene (PP) material exhibiting excellent fracture resistance and a universal commercial polymer that has extensively investigated from various aspects, including rheological properties, crystallization and melting behaviors, mechanical properties, and morphology behaviors.[1–5] IPC is usually produced via two-step polymerization: in the first stage, the homopolymerization of propylene is prepared, and then the second stage, the copolymerization of the ethylene and propylene is achieved.[6,7] Thus, it presents a multiphase structure and rubbery phase is a multilayered core–shell structure. The previous studies demonstrated that the dispersed rubbery phase consisted of four parts: ethylene–propylene multiblock copolymer (EbP) of ethylene-rich or propylene-rich, ethylene–propylene random copolymer (EPR), and a small amount of polyethylene homopolymer.[8–11] Morphological investigations indicated that the transition layer of EbP enhanced the interfacial adhesion between the dispersed phase and the matrix, which give the material excellent fracture resistance.[12,13]

Obviously, the multiphase morphology has great effect on the physical properties of the final products. The EbP exhibits a role of compatibilizer to enhance the interfacial adhesion between the dispersed phase and the matrix. Meanwhile, the core–shell structure was regarded as a modifier to offer the excellent toughness.[14] The enhanced toughness of IPC is mainly attributed to the multilayer structure of the dispersed rubber phase. It is known that the decrease of polymer rubbery phase particles size is beneficial to the improvement of toughness. Especially, PP blended with smaller elastomer particles exhibited higher toughness and much ductile property than those with larger particle size, probably because that suggested more efficient use of rubbery phase in promoting crazing and/or shear yielding of matrix.[15,16] However, a well-defined structure is influenced by some factors, such as a long-time thermal annealing.[12,17,18] Insufficient thermal processing and annealing time might result in an incomplete phase separation state.[19] In addition, the molten-state annealing at relatively high temperature destroyed the core–shell structure and induced an increase in the size of dispersed phase particles.[17] It is also reported that the destruction of the multiphase structure might cause a loss of the original excellent balance between toughness and rigidity of IPC.[20]

Recent works have been done to study the PP reinforced by varied elastomer in the existence of nucleating agent (NA).[21] It is expected that a certain amount NA is in favor of the morphology control of dispersed elastomer phase during the processing and finally affects the toughness of materials. Fanegas' work shown that the addition of NA caused a decrease of elastomer domain size in both PP/styrene-ethylene-butadiene-styrene and PP/poly olefin elastomer (POE) blends, and indeed increased the storage modulus and flexural modulus (FM) at the expense of a slight decrease in impact strength (IS) compared with binary blends.[22] Interestingly, Bai' s work suggested that the addition of certain amount NA provided great enhancement on the toughness of PP/POE blends without evident effect on the

Table I. Sample Characteristics of Virgin IPC Samples

Sample	M_w ($\times 10^5$ g/mol)	M_n ($\times 10^4$ g/mol)	M_w/M_n	Ethylene content (wt %)
IPC-A	2.07	3.90	5.32	6.0
IPC-B	1.94	3.72	5.25	4.5
IPC-C	1.87	3.67	5.10	4.0
IPC-D	2.28	4.26	5.34	3.5

morphology of elastomer phase.[23–25] The published inconsistent results indicated that much efforts are still required to fully understand the NA's function and the structure–property relationship. Therefore, the detailed investigation on how NA controls the particle size of the dispersed phase not only provide useful information to better understand the structure–property relationship of this material but also be helpful in designing and rationalizing of the processing technology.

In this work, we investigated the effect of α-form NA (NX8000) on the toughness of IPC. Bis-1,3-2,4-(4′propylbenzylidenyl)-1-propyl sorbitol (Millad® NX8000, Milliken Chemical), a member of sorbitol family,[26] was used in the study. The aim of this work is to figure out whether the NA is efficient in controlling the EPR phase size and enhancing the IS of IPC.

EXPERIMENTAL

Materials and Sample Preparation

Impact polypropylene copolymer (IPC) materials of different ethylene contents used in this study are produced by Beijing Research Institute of Chemical Industries, SINOPEC (Beijing, China). The ethylene contents of the samples were 6.0 wt %, 4.5 wt %, 4 wt %, and 3.5 wt % and were denoted as IPC-A, IPC-B, IPC-C, and IPC-D, respectively. The more characteristics of IPC of various ethylene contents used in this study are listed in Table I. The NA bis-1,3-2,4-(4′propylbenzylidenyl)-1-propyl sorbitol (NX8000, Milliken Chemical) was used as received. A small amount of antioxidant (Irganox 1010 and Irganox 168) was added to protect the thermal decomposition during melt processing.

Blends of IPC with various contents of ethylene and 0.3 wt % NX8000 were prepared using a corotating twin-screw extruder (ZSK-25, Germany) at barrel temperatures ranging from 230°C to 250°C. For convenience, the specimens with additive NX8000 were abbreviated as IPC-X, for example, IPC-A-X means IPC-A blend with 0.3 wt % NX8000.

Gel Permeation Chromatograph

Gel permeation chromatograph (GPC; Waters Alliance GPCV 2000) was used to measure the number-average molecular weight (M_n) and molecular weight (M_w) of samples. The solvent is 1,2,4-trichlorobenzene and polystyrene (Ps) was used as standard sample to calibrate the GPC. The flow rate for analysis was 1.0 mL/min with temperature maintained at 150°C. The concentration of sample for analysis is 1 mg/mL.

Mechanical Properties Measurements

The notched Izod IS of the specimens was tested with a VJ-40 Izod machine according to the ISO179-1:2010 standard. The IS was measured under room temperature (about 23°C), and the average value was reported from more than five specimens.

Microscope Analysis

A scanning electron microscopy (SEM) was used to observe the sample fractured surface with an acceleration voltage of 10 kV. Before observation, the injection-molded bar was first cryogenically fractured in two orthogonal directions that a fractured surface perpendicular to the flow direction (FD) and another perpendicular to the transverse direction (TD) showed in Figure 1. Then the fractured surface was etched by xylene at 60°C for 30 min to remove the EPR phase, then the etched surface was carefully washed with fresh xylene and coated with gold.[13,19]

The EPR particle size and size distribution were analyzed using Image Pro Plus software. Generally, each specimen was measured about 200 particles. The average particle size (d_n) and particle size distribution parameter (σ) are calculated by eqs. (1) and (2):

$$d_n = \frac{\sum_{i=1}^{N} n_i d_i}{\sum_{i=1}^{N} n_i} \tag{1}$$

$$\ln \sigma = \sqrt{\frac{\sum_{i=1}^{N} n_i (\ln d_i - \ln d_n)^2}{\sum_{i=1}^{N} n_i}} \tag{2}$$

where n_i represents the number of rubbery particles and d_i represents the diameter of rubbery particles.

Dynamic Mechanical Analysis

Dynamic mechanical analysis (DMA) testing was performed using a DMARSA III analyzer (TA Instruments).The three-point-bend mode was used, and the measurement was performed on a rectangular-shaped test part from 80 to 100°C at a heating rate of 3°C/min and an oscillatory frequency of 1 Hz. The test part with rectangular-shape was cut from the injection-

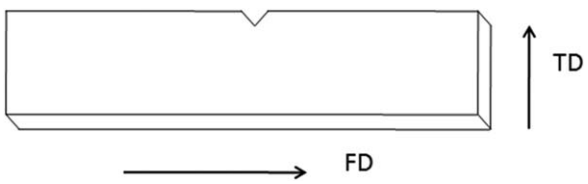

Figure 1. Schematic representation of the noticed injection mold used for cryogenic fracture in two orthogonal directions.

Table II. The Izod Notch IS at 23°C, FS, FM, and TS for Various Samples

	Samples							
	IPC-A	IPC-A-X	IPC-B	IPC-B-X	IPC-C	IPC-C-X	IPC-D	IPC-D-X
IS (kJ/m^2)	11.80	37.80	7.00	22.50	7.60	20.50	4.90	4.80
FS (MPa)	10.55	12.04	13.29	15.03	12.80	14.70	17.99	20.41
FM (GPa)	0.43	0.51	0.55	0.65	0.54	0.63	0.75	0.90
TS (MPa)	15.10	16.50	18.00	19.30	18.10	19.30	21.90	23.80

molded sample and it was adjusted to the size of 25 mm × 13 mm × 3 mm (length × wide × thickness).

Differential Scanning Calorimetry

The nonisothermal crystallization and melting of specimens were conducted on a Perkin-Elmer pyris-1 differential scanning calorimetry (DSC) instrument with nitrogen gas, calibrated by indium. The mass of test sample was about 5–10 mg. DSC scanning program was set as follows: first, the sample was heated from 50°C to 230°C at a heating rate of 10°C/min and maintained at 230°C for 5 min to erase the thermal history; subsequently, the sample was cooled down to 50°C at a cooling rate of 10°C/min, and second, heated to 230°C at a rate of 10°C/min. The crystallization thermograms were recorded during the first cooling scan, while the melting temperature and fusion enthalpy of the samples were determined during the second heating scan.

Wide-Angle X-ray Diffraction

Wide-angle X-ray diffraction (WAXD) was adopted to study the crystalline structure of PP matrix. WAXD patterns of the blends were obtained on a Bruker AXS D8 advance diffractometer with Ni-filtered Cu-Ka radiation ($\lambda = 0.154$ nm) under a voltage of 40 kV and a current of 250 mA. The scanning 2θ angle range used in this study is from 10° to 35°.

Rheology

A universal dynamic spectrometer (ARES, TA Instruments) was used to determine the rheological performance of IPC/NX8000 blends in the range 170–240°C under a nitrogen gas flow. The samples were heated to 240°C for 4 min to ensure complete

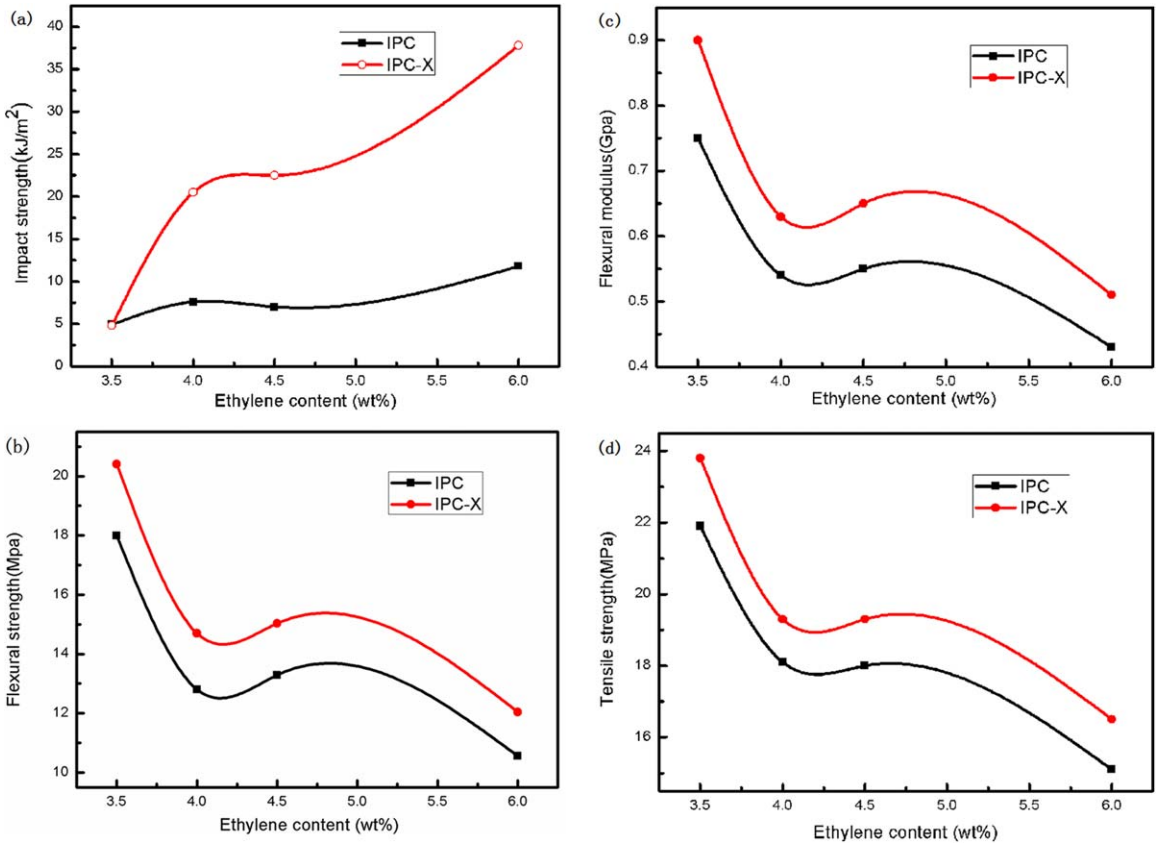

Figure 2. Variation of the mechanical properties versus the concentration of ethylene: (a) IS, (b) FS, (c) FM, and (d) TS. [Color figure can be viewed in the online issue, which is available at wileyonlinelibrary.com.]

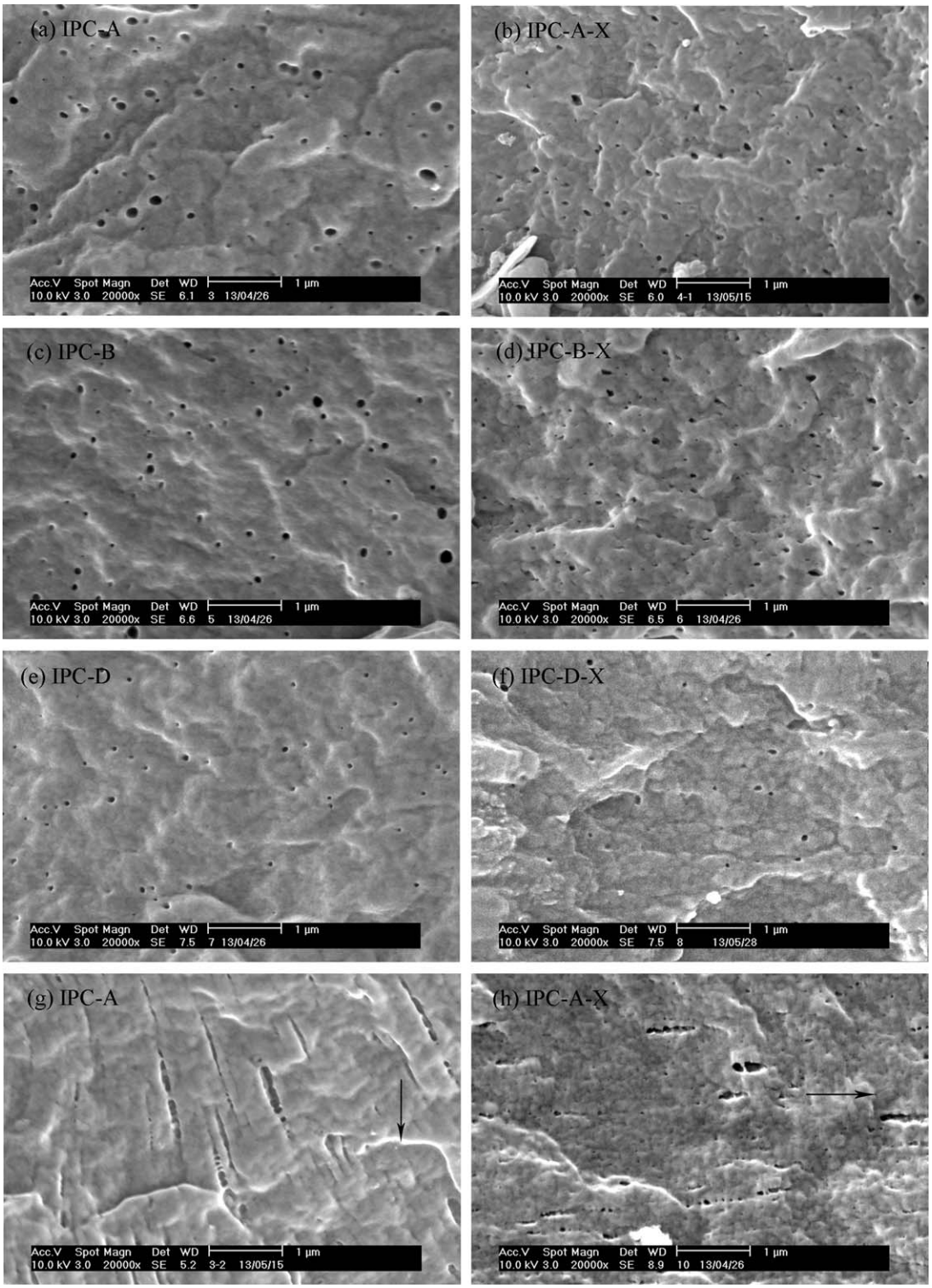

Figure 3. SEM micrographs of the dispersed particles from different directions (a)–(f) viewed parallel to FD; (g) and (h) viewed perpendicular to FD. Arrows point to FD.

melting of both IPC and NX8000 and subsequently cooled at a rate of 5°C/min. A 0.5% strain were imposed at a small amplitude oscillatory shear frequency of 10 rad/s. Specimens for rheological testing were compressed to a disk with a diameter of 25 mm and a thickness of 1 mm.

Polarized Optical Microscopy

Optical micrographs were taken on an Olympus AX70 polarized optical microscopy (POM) equipped with a Linkam THMS 600 hot stage under crossed polarizer. The samples were heated to 260°C and kept for 5 min to ensure complete melt as the

Table III. Results of DSC for IPC, the Average Dispersion Phase Size (d_n) and Size Distribution Parameter (σ) of IPC with and Without Addictive NX8000

Samples	T_c (°C)	T_p (°C)	ΔH_c (J/g)	d_n (μm)	σ
IPC-A	116.6	164.1	39.73	0.121	1.33
IPC-A-X	130.4	163.4	42.37	0.084	1.34
IPC-B	117.5	163,5	45.12	0.099	1.41
IPC-B-X	130.2	163.4	48.80	0.057	1.31
IPC-C	117.7	163.7	46.92	-	-
IPC-C-X	130.0	164.5	49.54	-	-
IPC-D	118.6	163.2	51.47	0.055	1.39
IPC-D-X	131.0	164.1	54.61	0.059	1.33

compression molded samples. Cooling rate used for the experiment is 10°C/min.

RESULTS AND DISCUSSION

Mechanical Properties

The mechanical properties of all specimens were investigated and the results are listed in Table II. Apparently, the IS, flexural strength (FS), and FM as well as tensile strength (TS) have been greatly improved by the addition of NX8000 except IPC-D. For example, the IS of IPC-A-X is enhanced to 37.8 kJ/m^2 at 23°C which is triple of IPC-A (11.8 kJ/m^2), indicating the apparent toughening effect of NX8000 for IPC. Meanwhile, the IS increases without a loss of rigidity compared with the origin IPC. IPC-B and IPC-C have the similar improvement in mechanical properties. However, compared with IPC-A, IPC-B, and IPC-C, the IS of IPC-D with the lowest ethylene content barely is changed, revealing that the content of ethylene also has effect on the mechanical properties of composites according to the brittle–ductile transition (BDT).

In polymer blends toughened by elastomers, normally there is a BDT, which is the sharp shift in the mode of failure from brittle fracture with poor toughness to ductile fracture with excellent toughness.[27–29] Figure 2 presents the effect of ethylene concentration on the mechanical properties of IPC. It can be observed that, with the addition of 0.3 wt % NX8000, the transition zone from brittle failure to ductile failure mainly occurred while the ethylene content varied between 3.5 wt % and 6 wt %. BDT is usually used to describe the deformation type and investigate the mechanical properties of materials for industrial applications. For IPC composites, the transition from brittle failure to ductile failure relates with the critical content of EPR and a critical distance between dispersed phase particles. With the increase of ethylene content, the content of rubbery phase increases accordingly. Once the content of rubbery phase is over the critical content and/or the interparticle distance is over the critical distance, the sample exhibits the largely increased IS. Obviously, the NA almost has no effect on the improvement of IS of composites while the ethylene content of IPC is less than 3.5 wt %. Conversely, it is well known that too much higher ethylene content also results in the decrease of other mechanical parameters. Thus, it can be proposed that the optimum condition for the addition of NA is that the ethylene content is in the transition zone.

Phase Morphology of EPR

To better understand the effect of NX8000 to the dispersed phase of the IPC composites, we used SEM to observe the multiphase morphology of samples. All the cross-sections of samples which were prepared by injection molding were etched by xylene for 30 min at 60°C to remove the EPR phase and then observed the two orthogonal fractured surfaces that one perpendicular to the FD in Figure 3(a-f) and another perpendicular to the TD in Figure 3(g,h). As shown in Figure 3, the dark holes or voids that can be observed in the fractured surfaces represented the EPR phase. It can be observed that the introduction of NA NX8000 caused visible size change of the dispersed phase in Figure 3(a-d). However, the morphologies of IPC-D shown in Figure 3(e,f) do not exhibit evident change on the size of dispersed phase by the addition of NX8000. The results for average size of dispersed phase (d_n) and size distribution parameter (σ) of IPC with and without addictive NX8000 are listed in Table III. The data reveal that the main reason of high improvement on material toughness is the decreased particle size of dispersed phase which controlled by the addition of NX8000. In other word, when the ethylene content is more than 3.5 wt %, the existence of NX8000 is beneficial to the morphology control of the dispersed phase during the process,

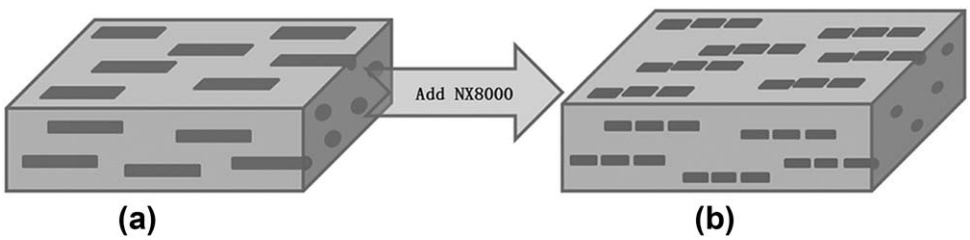

Figure 4. The schematic process of EPR phase change for IPC. (a) IPC without NX8000 and (b) IPC with NX8000.

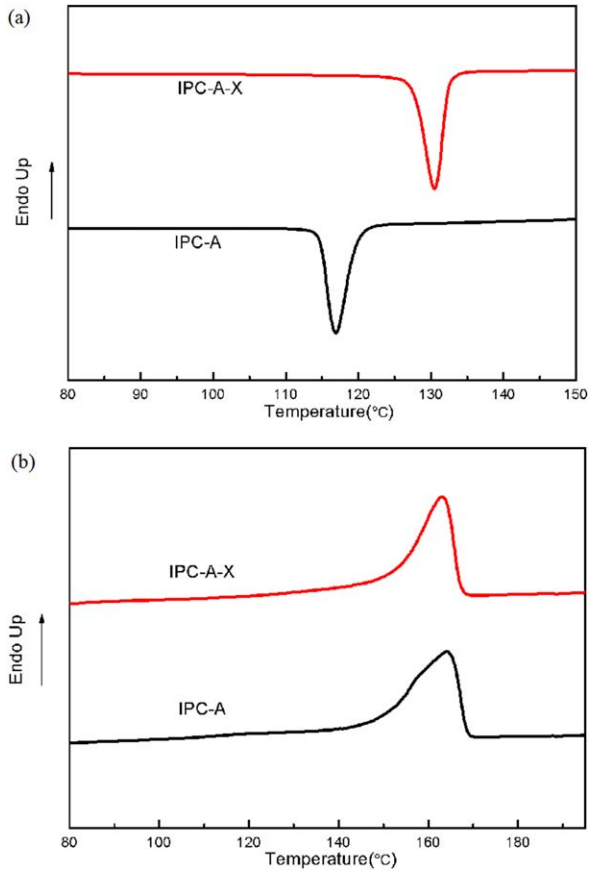

Figure 5. DSC thermograms of IPC-A and IPC-A-X (a) cooling and (b) subsequent heating, both at a rate of 10°C/min. [Color figure can be viewed in the online issue, which is available at wileyonlinelibrary.com.]

the particles size of EPR phase was became smaller with the addition of NX8000 (Figure 4). This result was consisted with Fanegas' work.

Crystallization Behavior of PP Matrix

DSC was used to investigate the crystallization behavior of the blends. The nonisothermal crystallization and melting curves of IPC-A and IPC-A-X samples are shown in Figure 5. The peak crystallization temperature (T_c) of IPC-A-X is 130.4°C, which is higher than that of IPC-A (116.6°C), indicating a strong nucleation effect of NX8000 for PP crystallization. Similarly, it can be observed that the peak crystallization temperature (T_c) of the other modified IPC produces an apparent increase compared to that of virgin IPC in Table III. Moreover, NA is able to reduce injection-molding cycles by raising the crystallization temperature and accelerating crystallization rate of semicrystalline.[24] Thus, the higher crystallization temperature and faster crystallization rate could affect the dispersed phase morphology of EPR through delaying the evolution of EPR phase up to equilibrium state during processing, and then influence the IS of IPC/NX8000 blends. Figure 5(b) shows that the shoulder in the melting peak of IPC-A was not apparent after the addition of NX8000 and the peak width was shrunk, suggesting the lamellae thickness of IPC-A-X become more uniform.

The melting temperature (T_p), crystallization temperature (T_c), and fusion enthalpy values (ΔH_c) for all the samples with and without NX8000 are summarized in Table III. It can be found that the addition of NX8000 do not show obvious influences on the T_p values of IPC (around 163–165°C), indicating only α-phase is formed during the cooling process. Moreover, the addition of NX8000 induces the slight increase of ΔH_c, confirming the NX8000 has a weak effect on crystallinity of PP matrix.

To better understand the effect of NX8000 on the matrix, the samples of IPC-A and IPC-A-X were analyzed by WAXD, and the results are displayed in Figure 6. The diffraction curves of IPC-A and IPC-A-X showed diffraction peaks at $2\theta = 14.1°$, 16.9°, 18.6°, 21.1°, and 21.8°, corresponding to the (110), (040), (130), (111), and (131) plane, represents the typical positions of α-crystalline of samples, further proves the results obtained from DSC analysis. It has been proved that for PP, the nucleating effect of bis(3,4-dimethylbenzylidene)-sorbitol (DMDBS) is greatly dependent on its content in the PP matrix. Above the critical content, DMDBS are more likely to form a fibril network structure with the fiber diameter of about 10 nm, which is very close to the lamellae thickness of PP.[30–34] Therefore, it exhibits evident nucleation effect for PP crystallization. In our work, it is clearly observed that NX8000 has great nucleation effect on PP crystallization. Thus, we proposed that the 0.3 wt % NX8000 can form the fiber network structure and much more details will be discussed in the following.

Dynamic Mechanical Analysis

To explore the relationship between fracture toughness and the molecular mobility in the amorphous phase, it can be deduced from mechanical relaxation, as shown in Figure 7, the modified process increases the storage modulus (G') values of specimens which relates to the improvement of crystallinity and crystalline structure.[35] It is intensively investigated from previous literatures that NA is widely used in semicrystalline polymer processing to control the crystallization behavior of such polymer greatly and induces the formation of spherulites with largely decreased diameters.[36–39] So this is why NAs are also thought to be one of the toughening reasons for PP.

It is particularly worth mentioning that the mechanical loss factor (tan δ) curves are thought to more useful to explain the

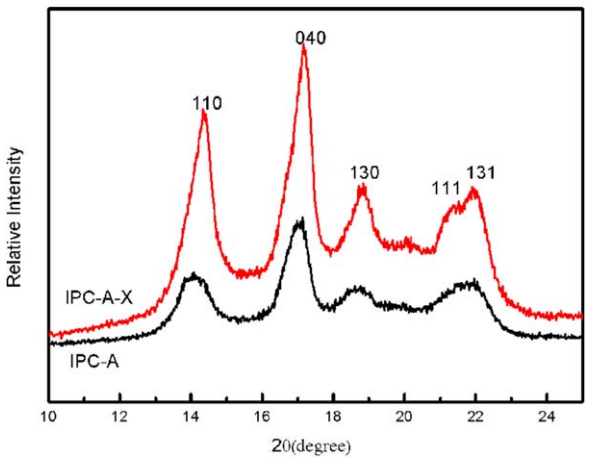

Figure 6. The WAXD spectra of IPC-A and IPC-A-X. [Color figure can be viewed in the online issue, which is available at wileyonlinelibrary.com.]

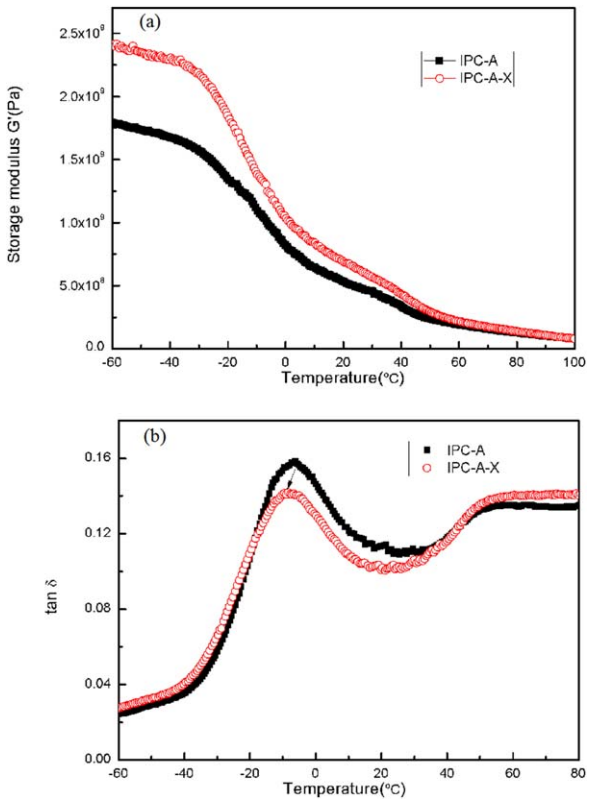

Figure 7. Storage modulus (G') and mechanical loss factor (tan δ) as a function of temperature for IPC-A and IPC-A-X. [Color figure can be viewed in the online issue, which is available at wileyonlinelibrary.com.]

toughness change.[40] The peak at about −10°C is the glass transition of unrestricted amorphous PP (T_g), while the peak at 60°C is related to α-relaxation, accounting for relaxation of restricted PP amorphous chains in the crystalline phase (defects), also known as rigid amorphous molecules.[41,42] Besides that, the T_g value of modified samples moves to lower temperature compared with that of unmodified samples, which is pointed out by arrow in Figure 6, indicating that the addition of NX8000 in PP melts promotes the mobility of amorphous chain segments. This can be ascribed to increase of crystallinity in the amorphous phase due to the second crystallization process relating to the change of some chain segments from amorphous state to crystalline state by the addition of NA.[35] This means that the chain interaction and mobility of the compounds in IPC/NX8000 blends are stronger than those of virgin IPC. So it is a favor of improving the IS by the addition of NX8000.

Rheology

Figure 8 shows the variation of the complex viscosity (η^*) with temperature for the IPC samples with various concentration of NX8000. Prior to the experiment, the sample was completely melted at 240°C for 4 min and were subsequently cooled at 5°C/min. For the neat IPC, η^* is observed to increase gradually with decreasing temperature, and it increases abruptly at 140°C. The dramatic increase in η^* ascribes to the solidification of PP matrix. Similar increases in η^* are evident in the other remaining curves, which correspond to the IPC with different concentrations of NX8000. It is worth noticing that the temperature at which this transition occurs are increased compared with that of neat IPC, confirming the expectation that NX8000 promotes the crystallization of PP matrix through nucleation at higher temperature.

In addition, the magnitude of the increase in η^* associated with the NX8000 is seen to increase with increasing the concentration of NA. This might caused by the generation and development of the NX8000 fibril network which is attributed to the corresponding phase separation and crystallization of NX8000. Therefore, it is also possible that shear is enhanced when the η^* of modified IPC increases than that of neat IPC in processing, which can prevent the evolution of EPR phase, and then affect the IS of IPC/NX8000 blends.

Polarized Optical Microscopy

POM was used to determine melting and crystallization transition in the IPC/NX8000 blends, especially for the NX8000. To further understand the fibrils structure, the sample of IPC blending with 5 wt % NX8000 and the mixture of IPC/1 wt % NX8000 are observed by POM, the former is easier to view the phenomena of phase separation. Figure 9(b1-b3) presents the morphologies of IPC/5 wt % NX8000, which were observed at different temperatures. The POM images of IPC/5 wt % NX8000 reveal the formed liquid–liquid phase separation at 260°C. In the further cooling process, phase-separated liquids, phase crystallization of NX8000 is observed when the temperature down to 240°C, at the same time, macroscopic fibrils are gradually generated and followed by the formation of fibril network in Figure 9(b2). By contrast, the POM observation of mixtures containing 1 wt % of NX8000 indicates that the melted sample exhibits homogeneous one-phase liquids in Figure 9(a1), and the fibril is almost invisible at 240°C, as shown in Figure 9(a2). Subsequently, it is obviously observed that the crystallization of PP matrix is occurred with the temperature down to 140°C in Figure 9(a3,b3). In previous work, it is reported that at very low contents, the additive

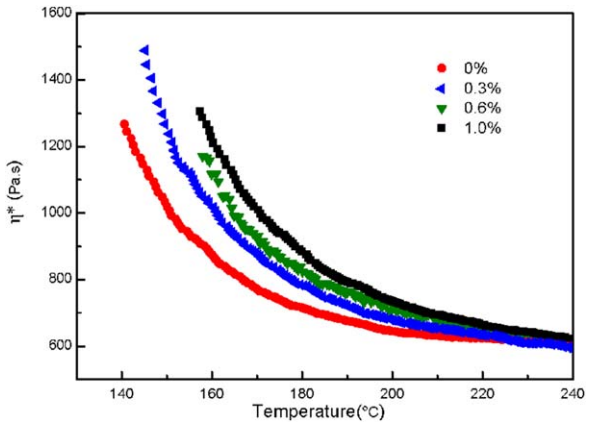

Figure 8. Complex viscosity (η^*) shown as a function of temperature upon cooling for the IPC at three different concentrations of NX8000. [Color figure can be viewed in the online issue, which is available at wileyonlinelibrary.com.]

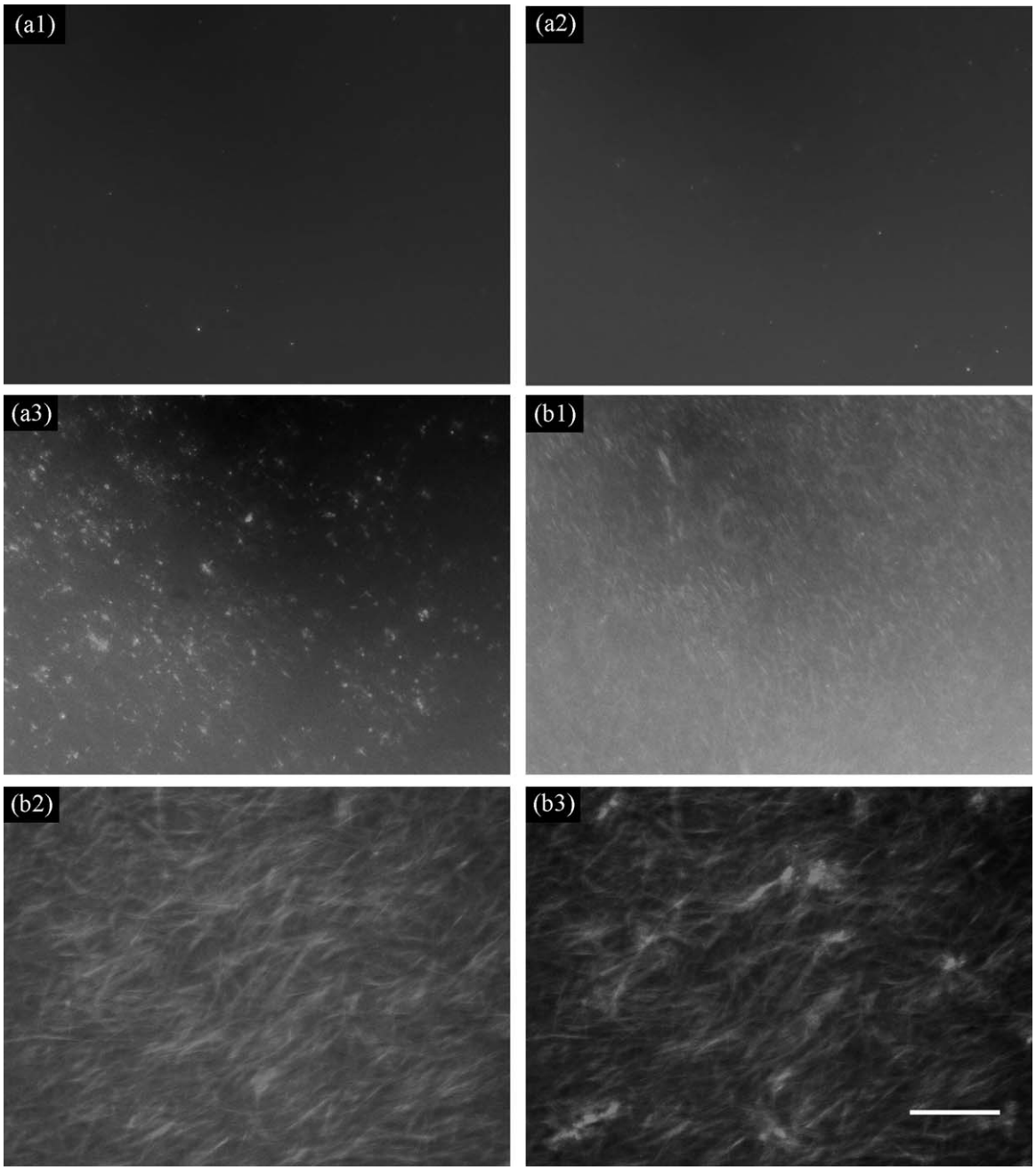

Figure 9. Optical micrograph of the binary IPC/NX8000 mixtures containing different amounts of NX8000 at various temperatures. (a1)–(a3) is 1 wt % NX8000 at 260°C, 240°C, and 140°C, respectively; (b1)–(b3) is 5 wt % NX8000 at 260°C, 240°C, and 140°C, respectively.

would be destruction by catalyst residues or "complete solubility."[43] Usually, the fibril network of samples with NX8000 concentration exceeding 2 wt % can be observed by optical microscopy.

CONCLUSIONS

In this work, α-NA NX8000 has been adopted to blend in a series of IPC samples with various ethylene contents. Compared with virgin IPC, the surprising enhancement in the impact toughness of modified IPC was achieved with improvement of the FS, FM, and TS. The results of SEM and POM suggested the formation of NA fibril network decreases the size of dispersion phase and makes the distribution uniform, indicating fibril network prevent the evolution of EPR phase and control the size of dispersed phase. DMA indicated the improvement of chain mobility is a favor of improving the IS. Therefore, our research provided an important way to produce the IPC material with excellent compressive mechanics.

ACKNOWLEDGMENTS

The authors thank the National Key Technology Support Program of China (2011BAE26B01) for supporting this work.

REFERENCES

1. Kontopoulou, M.; Wang, W.; Gopakumar, T. G.; Cheung, C. *Polymer* **2003**, *44*, 7495.
2. Yang, J.; Zhang, Y.; Zhang, Y. *Polymer* **2003**, *44*, 5047.
3. Pang, Y.; Dong, X.; Zhao, Y.; Han, C. C.; Wang, D. *Polymer* **2007**, *48*, 6395.
4. Meng, K.; Dong, X.; Zhang, X.; Zhang, C.; Han, C. C. *Macromol. Rapid Commun.* **2006**, *27*, 1677.
5. Pang, Y.; Dong, X.; Zhang, X.; Liu, K.; Chen, E.; Han, C. C.; Wang, D. *Polymer* **2008**, *49*, 2568.
6. Simonazzi, T.; Cecchin, G.; Mazzullo, S. *Prog. Polym. Sci.* **1991**, *16*, 303.
7. Galli, P.; Haylock, J. C. *J. Prog. Polym. Sci.* **1991**, *16*, 443.
8. Mirabella, F. M. *Polymer* **1993**, *34*, 1729.
9. Xu, J.; Feng, L.; Yang, S.; Wu, Y.; Yang, Y.; Kong, X. *Polymer* **1997**, *38*, 4381.
10. Zhu, H.; Monrabal, B.; Han, C. C.; Wang, D. *Macromolecules* **2008**, *41*, 826.
11. Dong, Q.; Wang, X.; Fu, Z.; Xu, J.; Fan, Z. *Polymer* **2007**, *48*, 5905.
12. Chen, Y.; Chen, Y.; Chen, W.; Yang, D. *Eur. Polym. J.* **2007**, *43*, 2999.
13. Chen, Y.; Chen, Y.; Chen, W.; Yang, D. *J. Appl. Polym. Sci.* **2008**, *108*, 2379.
14. Tan, H.; Li, L.; Chen, Z.; Song, Y.; Zheng, Q. *Polymer* **2005**, *46*, 3522.
15. Liu, Z.; Zhang, X.; Zhu, X.; Li, R.; Qi, Z.; Wang, F.; Choy, C. *Polymer* **1998**, *39*, 5019.
16. Jang, B.; Uhlmann, D.; Sande, J. V. *Polym. Eng. Sci.* **1985**, *25*, 643.
17. Chen, R.; Shangguan, Y.; Zhang, C.; Chen, F.; Harkin-Jones, E.; Zheng, Q. *Polymer* **2011**, *52*, 2956.
18. Svoboda, P.; Svobodova, D.; Slobodian, P.; Ougizawa, T.; Inoue, T. *Eur. Polym. J.* **2009**, *45*, 1485.
19. Zhang, C.; Shangguan, Y.; Chen, R.; Wu, Y.; Chen, F.; Zheng, Q.; Hu, G. *Polymer* **2010**, *51*, 4969.
20. Song, S.; Feng, J.; Wu, P.; Yang, Y. *Macromolecules* **2009**, *42*, 7067.
21. Fanegas, N.; Gomez, M.; Marco, C.; Jimenez, I.; Ellis, G. *Polymer* **2007**, *48*, 5324.
22. Fanegas, N.; Gomez, M.; Jimenez, I.; Marco, C.; Garcia-Martinez, J.; Ellis, G. *Polym. Eng. Sci.* **2008**, *48*, 80.
23. Bai, H.; Wang, Y.; Song, B.; Li, Y.; Liu, L. *J. Polym. Sci. Part B: Polym. Phys.* **2008**, *46*, 577.
24. Bai, H.; Wang, Y.; Song, B.; Han, L. *J. Appl. Polym. Sci.* **2008**, *108*, 3270.
25. Bai, H.; Wang, Y.; Song, B.; Huang, T.; Han, L. *J. Polym. Sci. Part B: Polym. Phys.* **2009**, *47*, 46.
26. Bernland, K.; Tervoort, T.; Smith, P. *Polymer* **2009**, *50*, 2460.
27. Jiang, W.; Liu, C.-H.; Wang, Z.-G.; An, L.-J.; Liang, H.-J.; Jiang, B.-Z.; Wang, X.-H.; Zhang, H.-X. *Polymer* **1998**, *39*, 3285.
28. Min, S. S.; Lee, S.-S.; Jho, J. Y. *J. Polym. Test.* **2001**, *20*, 855.
29. Liu, Z.; Zhang, X.; Zhu, X.; Qi, Z.; Wang, F.; Li, R.; Choy, C. *Polymer* **1998**, *39*, 5027.
30. Shepard, T. A.; Delsorbo, C. R.; Louth, R. M.; Walborn, J. L.; Norman, D. A.; Harvey, N. G.; Spontak, R. *J. Polym. Sci. Part B: Polym. Phys.* **1997**, *35*, 2617.
31. Nogales, A.; Mitchell, G. R.; Vaughan, A. S. *Macromolecules* **2003**, *36*, 4898.
32. Kristiansen, M.; Tervoort, T.; Smith, P. *Polymer* **2003**, *44*, 5885.
33. Lipp, J.; Shuster, M.; Terry, A. E.; Cohen, Y. *Langmuir* **2006**, *22*, 6398.
34. Li, X.; Wu, H.; Dai, J.; Huang, T.; Wang, Y. *J. Polym. Sci. Part B: Polym. Phys.* **2011**, *49*, 898.
35. Luo, F.; Wang, J.; Bai, H.; Wang, K.; Deng, H.; Zhang, Q.; Chen, F.; Fu, Q.; Na, B. *Mater. Sci. Eng. A* **2011**, *528*, 7052.
36. Feng, Y.; Jin, X.; Hay, J. *J. Appl. Polym. Sci.* **1998**, *69*, 2089.
37. Marco, C.; Ellis, G.; Gomez, M.; Arribas, J. *J. Appl. Polym. Sci.* **2002**, *84*, 2440.
38. Kotek, J.; Raab, M.; Baldrian, J.; Grellmann, W. *J. Appl. Polym. Sci.* **2002**, *85*, 1174.
39. Zhang, P.; Liu, X.; Li, Y. *Mater. Sci. Eng. A* **2006**, *434*, 310.
40. Grein, C.; Bernreitner, K.; Gahleitner, M. *J. Appl. Polym. Sci.* **2004**, *93*, 1854.
41. Boyd, R. H. *Polymer* **1985**, *26*, 1123.
42. Read, B. *Polymer* **1989**, *30*, 1439.
43. Kristiansen, M.; Werner, M.; Tervoort, T.; Smith, P.; Blomenhofer, M.; Schmidt, H.-W. *Macromolecules* **2003**, *36*, 5150.